




Facile fabrication of bimetallic Fe₂P–Ni₂P heterostructure for boosted oxygen evolution

Bing Liang¹, Xiaohui Hu¹, Dong Sun¹, Qun Yang^{1,3}, Huaibao Tang^{1,3}, Xueqin Zuo^{1,3}, Yunxiang Lin^{1,3}, and Guang Li^{1,2,3,*} 

¹ School of Physics and Materials Science, Institute of Physical Science and Information Technology, Anhui University, Hefei 230601, China

² Key Laboratory of Structure and Functional Regulation of Hybrid Materials of Ministry of Education, Anhui University, Hefei, China

³ Anhui Key Laboratory of Information Materials and Devices, Anhui University, Hefei, China

Received: 24 May 2021

Accepted: 12 August 2021

Published online:
21 August 2021

© The Author(s), under exclusive licence to Springer Science+Business Media, LLC, part of Springer Nature 2021

ABSTRACT

Developing high-efficient yet low-cost electrocatalysts is crucial for the electrochemical oxygen evolution reaction (OER). Here a universal strategy for the facile synthesis of bimetallic Fe₂P–Ni₂P heterostructure has been developed. And the catalytic activity of the obtained bimetallic heterostructure had further studied. The sample was obtained by hydrothermal method through mixing the nickel–iron precursors followed by direct phosphating annealing. The catalyst has flower ball morphology that provides a massive active surface area with more active sites. At the same time, the Fe₂P–Ni₂P bimetallic heterostructure sample has excellent OER catalytic performance under alkaline electrolyte with an overpotential of 317 mV to achieve the current density of 10 mA cm^{−2} in 1.0 M KOH solution and a low Tafel slope of 58.71 mV dec^{−1}. This research proposes a general and economical method for the preparation of heterogeneous metal phosphide electrocatalysts toward the OER.

1 Introduction

The increasing environmental pollution and the over-exploitation of the earth's resources call for further development of clean energy to replace the fossil energy. Electrochemical water splitting is considered as a promising way to produce clean and sustainable hydrogen energy [1, 2]. Oxygen evolution reaction (OER) is a magnitude procedure in the electrochemical water splitting process and is one of the hinge factors affecting hydrogen efficiency of electrolytic

aquatic products [3]. The typical OER process involves four sequential proton-coupled electron transfers, leading to the large overpotentials to overcome the kinetic barrier [4]. Therefore, the progress of a highly efficient and low-price oxygen evolution catalyst could quicken up the inherent reaction kinetics and reduce the overpotential of OER, further enhancing the productivity of electrochemical water splitting. At present, noble metal (e.g., Ru, Ir, and Pt)-based catalysts are recognized as the most effective catalysts for hydrogen production

Address correspondence to E-mail: liguang1971@ahu.edu.cn

among various electrocatalysts [5, 6]. However, the limited inventory and high price still hinder its large-scale industrial application [7–9]. Thus, exploiting new class of electrocatalysts and revealing the catalytic mechanism are of great significance for the rapidly growing demand toward oxygen evolution.

As a promising alternative OER electrocatalysts, the earth-abundant transition metal phosphides, have given rise to follow with more interest in recent years [10–14]. The phosphorus in the phosphide structure can participate in the reaction through moderate bonding with the reaction intermediates, thus forming active sites with proton receptors and hydride receptors on its surface [15]. Most of all the heterogeneous bimetallic phosphides as OER or bifunctional electrocatalysts have attracted widespread attention, including Fe–CoP [16], $(\text{Ni}_{0.33}\text{Fe}_{0.67})_2\text{P}$ [17], FeP/Ni₂P [18], and FeCo/Co₂P [19], due to their chemical advantages and various structural properties [20–22]. Previous studies have demonstrated that the OER properties of nickel phosphate and iron phosphate were because of the synergetic effect of Fe³⁺ and Ni³⁺ in the catalyst. Because their lower coordination number and higher H₂O adsorption energy can induce OOH* deprotonation to produce O₂, they are proved as the active centers of OER [23, 24]. Designing and fabricating the dual metal Ni and Fe compounds are significant for oxygen evolution reaction.

Here, we advance a tactics to synthesize supportless Fe₂P–Ni₂P bimetallic heterostructure electrocatalyst (FNP). The Ni–Fe precursor has been uniformly mixed by hydrothermal synthesis and then the Fe₂P–Ni₂P sample was obtained by direct phosphating annealing. The flower-like morphology of the catalyst reveals a lot of active surface area, and these more active sites lead to high active material loading mass and excellent electrocatalytic efficiency [25]. The active substances Ni/Fe-oxide or Ni/Fe-hydroxide formed on the surface after the OER of bimetallic phosphides have excellent desorption ability to the intermediate (O*, OH*, and OOH*) [7, 26]. And the internal Fe₂P–Ni₂P core has better conductivity and a higher transfer coefficient, resulting in a synergistic effect in improving the catalytic performance [22, 27]. The special Fe₂P–Ni₂P bimetallic heterojunction was bond by the interaction between Fe₂P and Ni₂P lattice. And this catalyst shows excellent OER activity and stability, with an overpotential of 317 mV at a current density of 10 mA cm⁻² and a low Tafel slope

of 58.71 mV dec⁻¹ in 1.0 M KOH solution. In addition, FNP has a stable OER catalytic ability that for more than 20 hours. This work mainly studies the improvement of heterojunctions in double transition metal phosphates for catalytic efficiency. And the mend of Ni–Fe bimetal phosphates binding mode makes the OER electrocatalytic material with a good appearance and catalytic properties without using foam nickel and MOF or carbon cloth. This pioneering work opens a new path for designing a bimetallic phosphate as a catalyst for OER and other applications.

2 Experimental details

2.1 Materials

Nickel acetate (98.0%), Iron nitrate nonahydrate (98.5%), and Potassium hydroxide (KOH, > 85%) were purchased from Shanghai Macklin Biochemical Co., Ltd. Hexamethylenetetramine (HMT) was purchased from Sinopharm Chemical Reagent Co., Ltd. Nafion solution (5 wt%) were purchased from Alfa Aesar. Carbon fiber paper (thickness: 3 mm) was purchased from Shanghai Hesen electric co., Ltd. Anhydrous ethanol purchased from Cologne Chemical Products Co., Ltd. All the reagents and chemicals were not further purified before use.

2.2 Synthesis of Fe₂P–Ni₂P(FNP), Ni₂P, and Fe₂P

In a typical preparation of FNP, 0.5 mmol Iron (III) nitrate anhydrous, 1.5 mmol nickel acetate, and 4 mmol hexamethylenetetramine (HMT) were dissolved in 40 mL deionized water under uniform stirring. Then the uniform mixture was transferred to a 100 mL Teflon-lined autoclave and went through a hydrothermal reaction at 120 °C for 12 h. After cooling down to room temperature, the precipitate was collected by centrifugation and washed with deionized water and ethanol three times, respectively. The resulting precipitate was dried in an oven at 70 °C and ground to fine powder before annealing. Then the obtained Ni–Fe precursor and 1.0 g of red phosphorus were put into two ceramic boats, respectively, inside a tube furnace and ensuring that the red phosphorus was situated upstream. After flushed with N₂ for 30 min to get rid of the air in the quartz

tube, the temperature at the center of the furnace was elevated to 500 °C and maintained at 500 °C for 4 h at a ramping rate of 5 °C per minute. Then naturally cooled down to ambient temperature and the final product was obtained. The Ni₂P and Fe₂P were prepared by adding only nickel acetate and Iron (III) nitrate anhydrous in the first step with the remaining steps unchanged.

2.3 Materials characterization

To identify the crystal structure and chemical composition of the as-prepared samples, X-ray diffraction (XRD) data were collected with a Cu K α radiation ($\lambda = 0.15406$ nm) source. X-ray photoelectron spectrometry (XPS) was carried out on an ESCALAB250Xi spectrometer with monochromatic Al K α radiation to confirm the elemental constituents and bonding configurations. Scanning electron microscopy (SEM; Hitachi S-4800, Japan) and transmission electron microscopy (TEM; JEOL, JEM-2100SX, Japan) were used to monitor the microstructures of the samples.

2.4 Electrochemical characterizations

All electrochemical measurements were performed using a three-electrode system on a CHI760e workstation (Shanghai Chenhua, China) at room temperature. The mixture of 5 mg synthetic catalyst, 800 μ L water, 200 μ L ethanol, and 50 μ L 5 wt% Nafion solution was dispersed using ultrasonic to prepare catalyst ink. Then the catalyst ink of 5 μ L was uniformly dripped on the surface of the polished glassy carbon electrode (GCE, diameter 3 mm) and dried in the air as the working electrode. Hg/HgO electrode as the reference electrode and Pt plate as the counter electrode. 1.0 M KOH solution (99.99% metal purity) was used as an electrolyte and oxygenated for 30 min before each test to achieve O₂-saturated. All potentials were iR-corrected to compensate for the effect of solution resistance (80% solution resistance). All electrochemical potentials in this paper were calibrated to reversible hydrogen electrode (RHE) potentials according to the Nester equation ($E_{\text{RHE}} = E_{\text{Hg}/\text{HgO}} + 0.098 + 0.059 \times \text{pH}$) and the overpotential (η) of the OER was calculated as follows: η (V) = $E_{\text{RHE}} - 1.23$ V.

3 Results and discussion

3.1 Characterization and morphology

In this study, the bimetallic Fe₂P–Ni₂P phosphide catalyst has been prepared by hydrothermal and annealing phosphating. Firstly, uniformly mixed Ni–Fe precursors were obtained by the hydrothermal method. After drying and grinding at 70 °C in the oven, the Ni–Fe precursor and red phosphorus were put into a tubular furnace and annealed at 500 °C for 4 h under nitrogen atmosphere with the heating rate of 5 °C min^{−1}. Meanwhile, Ni₂P and Fe₂P were synthesized by phosphating separately as a comparison. The crystal structure of the samples was determined by powder X-ray diffraction (XRD) analysis, as shown in Fig. 1a; the FNP sample has five broad peaks at 30.5° (110), 47.4° (210), 52.9° (002), 54.2° (300), and 54.7° (211) belonging to Fe₂P (JCPDS 76-0089), while those have five broad peaks at 40.8° (111), 44.7° (021), 47.3° (210), 54.2° (300), and 54.4° (002) belong to Ni₂P (JCPDS 65-9706). This fully indicates that the Ni and Fe-mixed precursor was transferred to the heterostructure of Ni₂P and Fe₂P. The results of XRD spectra of Ni₂P and Fe₂P as contrast samples are also consistent with Ni₂P (JCPDS 65-9706) and Fe₂P (JCPDS 76-0089) cards to prove the successful synthesis of Ni₂P and Fe₂P.

The specific morphology and structural characteristics of the FNP sample are analyzed using field emission scanning electron microscopy (SEM) and transmission electron microscopy (TEM). It can be seen from Fig. 1b and c that the precursors of Ni₂P and Fe₂P are evenly mixed by the hydrothermal method and the flower-like spherical morphology is formed by phosphating. This structure can provide a large of active surface areas and expose the active sites to the maximum extent, thus promoting the improvement of electrocatalytic performance. The corresponding TEM images (Fig. 1d, e) show that the FNP heterostructure has clear and visible lattice stripes with the crystal plane spacing of 0.126 nm and 0.2 nm, corresponding to the (400) and (201) crystal planes of Ni₂P and Fe₂P, respectively. In addition, the heterostructure in the phase boundary region between Ni₂P and Fe₂P phase marked in Fig. 1e can prove that the heterostructure between Ni₂P and Fe₂P is formed after phosphating, and the interface bonding effect generated by this heterostructure is conducive to exposing more active sites [20, 21],

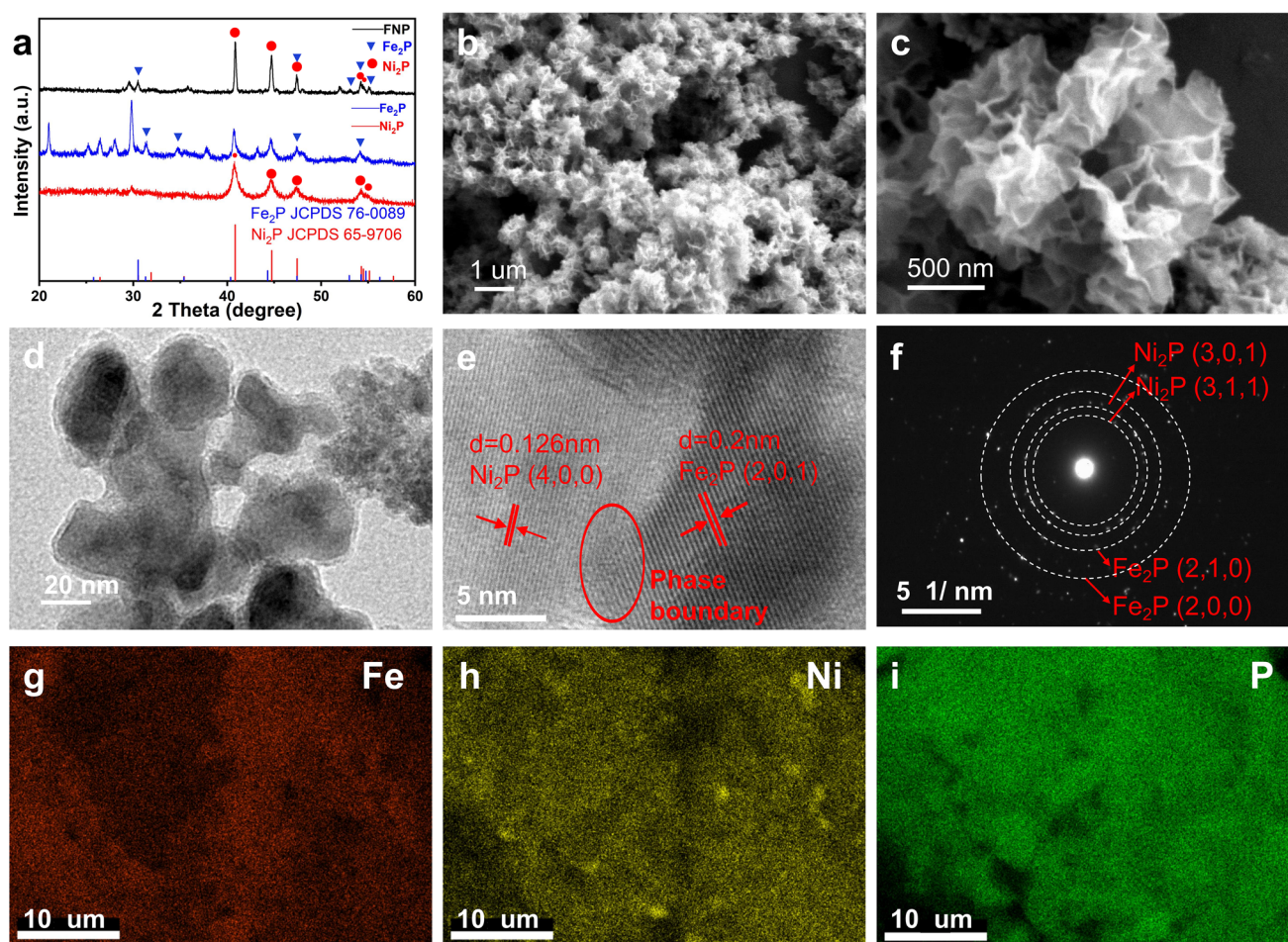


Fig. 1 a XRD patterns of FNP/Ni₂P/Fe₂P. b, c SEM and d TEM images of FNP. e HRTEM images and f SAED pattern of FNP. g–i EDX mapping of FNP

promoting charge transfer and thus promoting the reaction kinetics. The ring pattern from selected area electron diffraction (SAED) shown in Fig. 1f reveals that the characteristic (210) and (200) belong to the Fe₂P and the (301) and (311) belong to the Ni₂P, which match well with the XRD results. Moreover, according to the energy-dispersive X-ray spectrometry (EDX) mapping images in Fig. 1g–i illustrate the uniform distribution of Ni, Fe, and P elements in FNP sample. The result shows that the P element has sufficient combination with Fe and Ni in the phosphating process. The results of XRD and TEM analysis proved the successful synthesis of the FNP heterostructure.

3.2 Electrochemical properties

The electrocatalytic OER performance of FNP in alkaline solution was studied using a standard three-

electrode system. Ni₂P and Fe₂P were tested under the same conditions as the contrast. Prior to the linear sweep voltammetry (LSV) test, the samples were subjected to several cyclic voltammetry (CV) cycles in the electrolyte at a scan rate of 100 mV S⁻¹ until a stable CV curve was obtained. The LSV curves of the samples were obtained at a scan rate of 10 mV s⁻¹ with 90% iR-compensation [28]. The obtained LSV activation performance curves are shown in Fig. 2a. FNP sample electrocatalysts exhibit better catalytic activity with an overpotential of 317 mV at 10 mA cm⁻¹ current density significantly smaller than that of Ni₂P (365 mV) and Fe₂P (600 mV), indicating that the heterojunction bimetallic phosphide synthesized by phosphating can significantly enhance the OER activity. Tafel slope, which describes the effect of potential or overpotential on steady-state current density, is a key factor in evaluating OER dynamics. Using the LSV curve in Fig. 2a

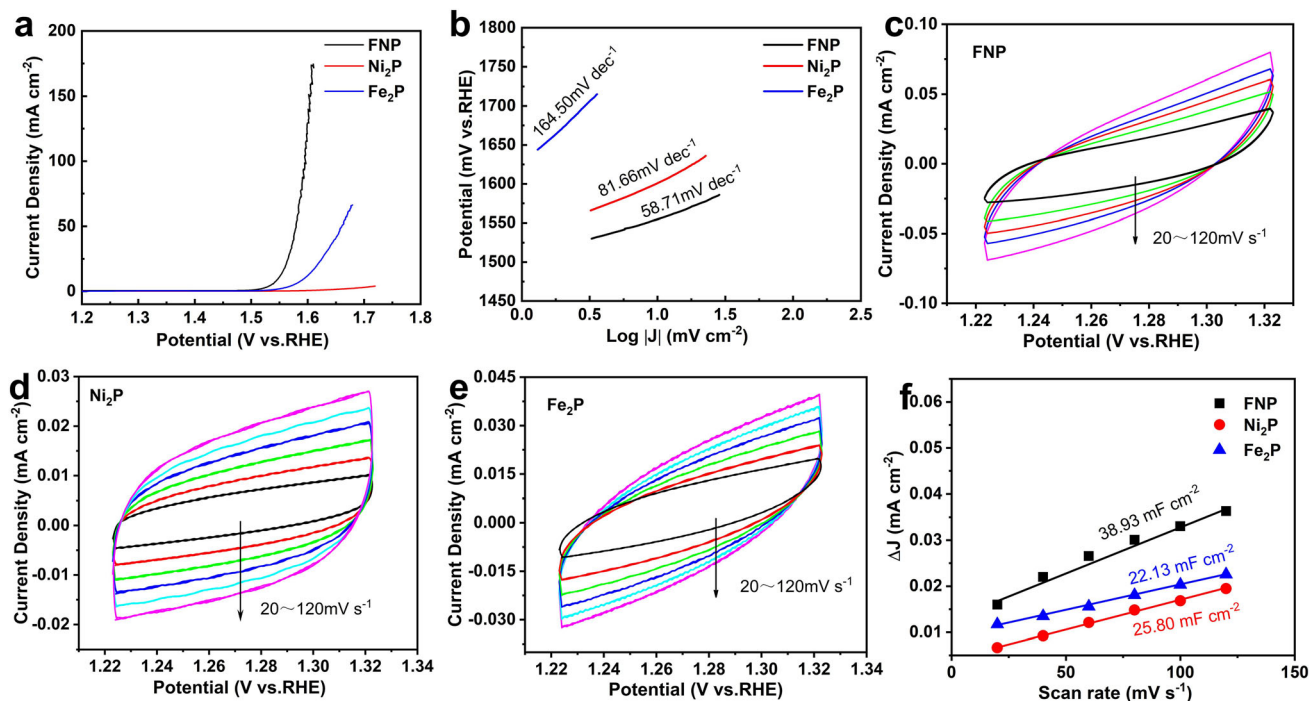


Fig. 2 **a** OER LSV curves of FNP, Ni₂P, and Fe₂P samples in 1.0 M KOH electrolyte. **b** Tafel plots derived from the polarization curves in (a). CV curves for **c** FNP, **d** Ni₂P, and **e** Fe₂P at different

scan rates: 20, 40, 60, 80, 100, and 120 mV s⁻¹ from inside to outside. ($\Delta j_0 = \Delta j_{ia} - \Delta j_{ic}$). **f** Capacitive currents at 1.25 V (vs RHE) as a function of the scan rate for FNP, Ni₂P, and Fe₂P

to calculate the Tafel slope of the corresponding sample, as shown in Fig. 2b, and the Tafel slope of the FNP shown in Fig. 3b is 58.71 mV dec⁻¹ which is much lower than those of Ni₂P (81.66 mV dec⁻¹) and the Fe₂P (164.50 mV dec⁻¹), which indicates that the heterojunction formed by the metal phosphide of Fe-Ni has a faster electron transfer speed and enhances the electrocatalytic kinetics of FNP [29, 30].

Since the electrochemical active surface area (ECSA) is proportional to the double-layer capacitance (C_{dl}), the intrinsic surface area activity of the sample is evaluated by ECSA as shown in Fig. 2b–d

[31]. The C_{dl} of the FNP sample is the largest among the three samples (38.93 mF cm⁻²), compared with Ni₂P (25.80 mF cm⁻²) and Fe₂P (22.13 mF cm⁻²), which means that the heterostructure of Ni₂P and Fe₂P in the FNP sample produced a larger electrochemical active region with more active sites [32].

The electrochemical impedance in Fig. 3a shows that the FNP sample has lower impedance than that of Ni₂P and Fe₂P, indicating that the FNP sample has a higher charge transport rate and better OER catalytic activity, which also proves that the Ni₂P–Fe₂P heterostructure can improve the conductivity. The

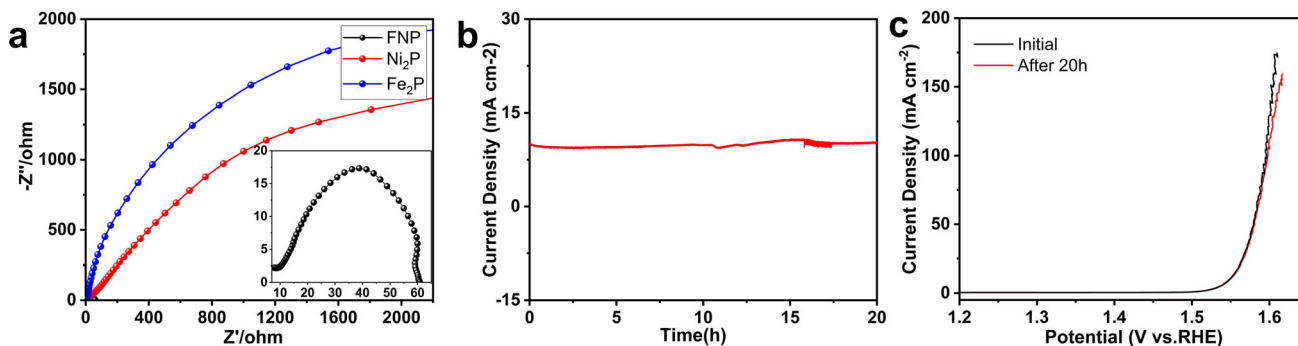


Fig. 3 **a** Nyquist plots of FNP, Ni₂P, and Fe₂P samples. **b** Chronopotentiometry curves at a constant current density of 10 mA cm⁻² for FNP. **c** LSV curves before and after 20-h CV cycles for FNP

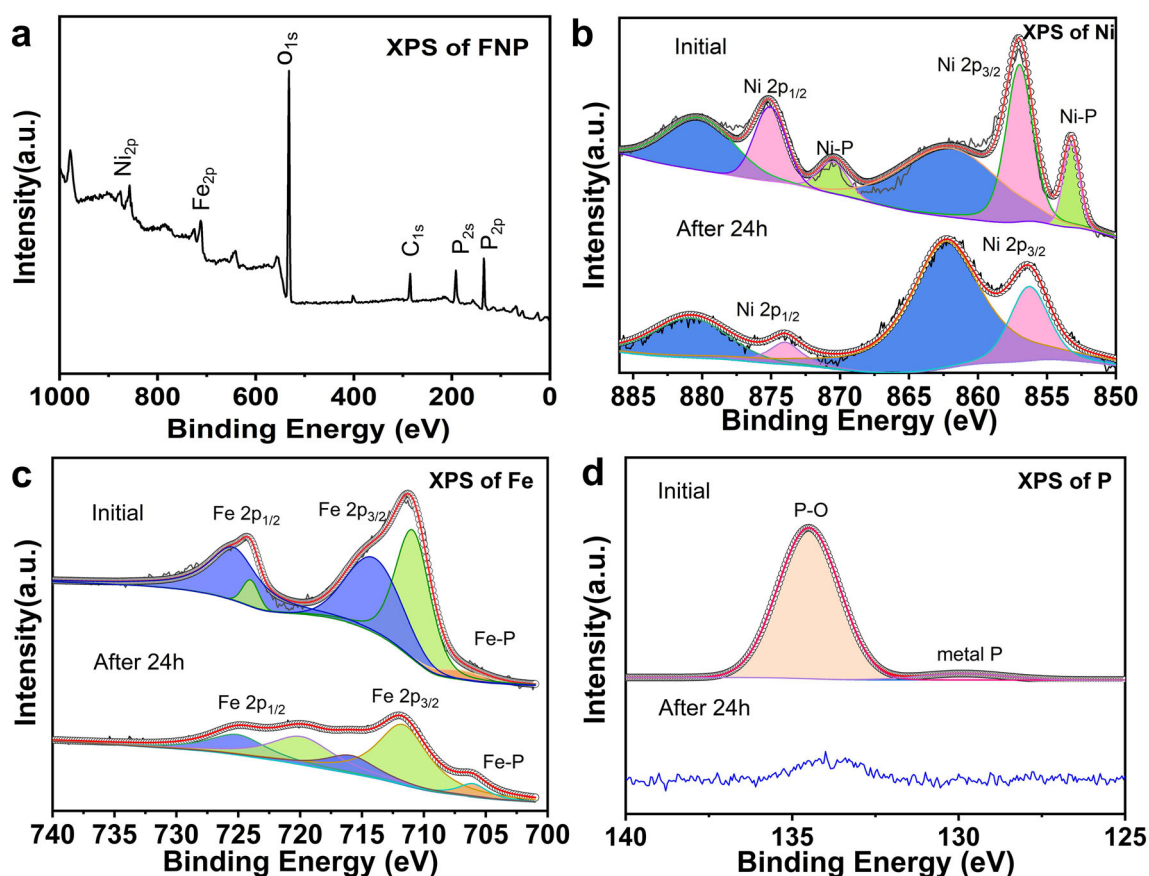


Fig. 4 a Overall XPS spectra of FNP. High-resolution XPS spectra of b Ni and c Fe. d P in FNP before and after OER electrolysis in 1.0 M KOH

durability and stability of FNP were tested by scanning the FNP electrode with a continuous CV cycle at 100 mV s^{-1} scanning rate and constant current density at 10 mA cm^{-2} . As shown in Fig. 3b, the over-potential required to produce the same current density after 20 h of CV cycle does not significantly decrease, indicating that the FNP sample has excellent anti-aging catalytic activity.

In order to further confirm the formation of bimetallic phosphides and investigate the effect of Fe_2P and Ni_2P heterostructures on the catalytic efficiency of electrocatalytic water splitting, the valence of FNP samples before and after OER test had been analyzed by X-ray photoelectron spectroscopy (XPS) analysis. The FNP overall XPS spectra (Fig. 4a) showed obvious elemental Ni, Fe, and P signals, consistent with the sample's XRD and EDX mapping data. The nickel elements before the OER test had four peaks in the 2p spectrum (located in Fig. 4b). The peaks at 853.2 eV and 870.9 eV can be indexed to Ni–P bonds, and the peaks at 856.9 eV and 875.0 eV

correspond to the Ni^{3+} in the Ni–O bond attributed to the oxidation of the FNP surface [33, 34]. The peaks at 861 eV and 880.19 eV belong to satellite peaks. In comparison, the Ni–P bond peaks at 853.2 eV and 870.9 eV of FNP samples disappeared after the test, which indicated that the Ni–P bond in Ni_2P decomposed and formed Ni–O/OOH phase catalytic active sites on the surface. For the Fe 2p spectrum of initial FNP (Fig. 4c), the peak located at 706.3 eV corresponds to the Fe–P bond, indicating the formation of Fe_2P . The peaks of Fe $2p_{3/2}$ and Fe $2p_{1/2}$ appearing at 711.3 eV and 724.2 eV belong to Fe^{2+} , respectively. While the peak values of 714.4 eV and 725.6 eV with higher binding energies correspond to the Fe^{3+} in iron oxide because of the surface oxidation of iron phosphides in the air [35, 36]. It can be observed that the double peaks from Fe^{2+} in FNP samples after OER operation become weakened and the double peaks from Fe^{3+} are enhanced [37], which indicate that Fe^{2+} is oxidized to a higher valence state after OER operation, forming Fe–O/OOH, which further

promotes the enhanced OER activity. In Fig. 4d, the initial samples show two peaks of P 2p. The peak at 130.0 eV belongs to the P 2p of the P-metal species. The other one peak at 134.5 eV corresponds to the oxidized P species peaks of the disappearance of two peaks after OER reaction which indicates that the phosphides FNP by stability test decompose into metal hydroxides to form a new Ni/Fe oxygen hydroxide–phosphide interface, which can overcome the disadvantage of poor conductivity of hydroxyl hydroxides.

Based on the above results, the catalytic performance of heterogeneous structure FNP was improved, mainly due to the following factors: 1. the flower-like morphology gives the catalyst more active surface area and active sites to enhance the transfer of electrons. 2. The interface bonding effect of heterostructure leads to the appearance of cations with a more complex electronic structure and higher conductivity, which reduces the thermodynamic barrier of the 4 e multiproton-coupled electron transfer step and promotes the formation of O–O bond, thereby improving the electrocatalytic efficiency [38]. 3. In the OER reaction, FNP heterojunction forms an interface of Ni(Fe) oxyhydroxide/phosphate on the surface. This hybrid interface has good adsorption capacity for intermediates (O^* , OH^* , and OOH^*) and thus greatly enhances the electrocatalytic efficiency [7, 39]. Therefore the synergy brought about by the heterostructure between the rich Ni₂P and Fe₂P interfaces and the formed Ni(Fe)–O/OOH surface layer gives NFP electrode superior activity and stability.

4 Conclusion

As mentioned above, a new type of Ni₂P–Fe₂P bimetallic heterostructure phosphide composite was obtained by phosphating Ni–Fe-mixed precursors directly in N₂, which was used as a catalyst for OER electrolytic water. The bimetallic phosphide heterojunction of this material shows high electrodynamics and enhanced conductivity. Meanwhile, the synergistic interaction between Ni₂P and Fe₂P-rich interfaces and the formation of Ni/Fe-oxyhydroxide surface layer contributes to the superior electrocatalytic performance and working stability of the FNP. FNP's excellent OER electrolytic water properties indicate that this pioneering work opens a new path

for designing bimetallic phosphides as catalysts for water electrolysis and other applications.

Acknowledgements

This work was financially supported by National Key R&D Program of China (2017YFA0403503), National Natural Science Foundation of China (11674001), Open Fund for Discipline Construction, Institute of Physical Science and Information Technology (S01003103, Anhui University), the Doctoral research start-up funds projects of Anhui University (J01003201), Leading Talent Innovation Team of Anhui Province (LTIT20200002), and the Key Projects of Natural Science Research in Universities of Anhui Province (KJ2020A0018).

References

1. I. Staffell, D. Scamman, A. Velazquez-Abad, P. Balcombe, P.E. Dodds, P. Ekins, N. Shah, K.R. Ward, The role of hydrogen and fuel cells in the global energy system. *Energy Environ. Sci.* **12**, 463–491 (2019)
2. C.G. Morales-Guio, L.A. Stern, X. Hu, Nanostructured hydrotreating catalysts for electrochemical hydrogen evolution. *Chem. Soc. Rev.* **43**, 6555–6569 (2014)
3. K. Zeng, D. Zhang, Recent progress in alkaline water electrolysis for hydrogen production and applications. *Prog. Energy Combust. Sci.* **36**, 307–326 (2010)
4. J. Masud, A.T. Swesi, W.P.R. Liyanage, M. Nath, Cobalt selenide nanostructures: an efficient bifunctional catalyst with high current density at low Coverage. *ACS Appl. Mater. Interfaces.* **8**, 17292–17302 (2016)
5. G. Chen, T. Wang, J. Zhang, P. Liu, H. Sun, X. Zhuang, M. Chen, X. Feng, Accelerated hydrogen evolution kinetics on NiFe-layered double hydroxide electrocatalysts by tailoring water dissociation active sites. *Adv. Mater.* **30**, 1–7 (2018)
6. C. Xiao, J. Zhang, Architectural design for enhanced C₂ product selectivity in electrochemical CO₂ reduction using Cu-based catalysts: a review. *ACS Nano* **15**, 7975–8000 (2021)
7. Y. Li, Z. Dong, L. Jiao, Multifunctional transition metal-based phosphides in energy-related electrocatalysis. *Adv. Energy Mater.* **10**, 1–36 (2020)
8. Z. Lin, B.B. Xiao, Z. Wang, W. Tao, S. Shen, L. Huang, J. Zhang, F. Meng, Q. Zhang, L. Gu, W. Zhong, Planar-coordination PdSe₂ nanosheets as highly active electrocatalyst for hydrogen evolution reaction. *Adv. Funct. Mater.* **2**, 2102321 (2021)

- L. Zheng, S. Han, H. Liu, P. Yu, X. Fang, Hierarchical MoS₂ nanosheet@TiO₂ nanotube array composites with enhanced photocatalytic and photocurrent performances. *Small* **12**, 1527–1536 (2016)
- G.F. Chen, T.Y. Ma, Z.Q. Liu, N. Li, Y.Z. Su, K. Davey, S.Z. Qiao, Efficient and stable bifunctional electrocatalysts Ni/Ni_xM_y (M = P, S) for overall water splitting. *Adv. Funct. Mater.* **26**, 3314–3323 (2016)
- J.D. Costa, J.L. Lado, E. Carbó-Argibay, E. Paz, J. Gallo, M.F. Cerqueira, C. Rodríguez-Abreu, K. Kovnir, Y.V. Kolenko, Electrocatalytic performance and stability of nanostructured Fe-Ni pyrite-type diphosphide catalyst supported on carbon paper. *J. Phys. Chem. C* **120**, 16537–16544 (2016)
- S.H. Ahn, A. Manthiram, Direct growth of ternary Ni-Fe-P porous nanorods onto nickel foam as a highly active, robust bi-functional electrocatalyst for overall water splitting. *J. Mater. Chem. A* **5**, 2496–2503 (2017)
- Y. Feng, X.Y. Yu, U. Paik, Formation of Co₃O₄ microframes from MOFs with enhanced electrochemical performance for lithium storage and water oxidation. *Chem. Commun.* **52**, 6269–6272 (2016)
- A. Dutta, N. Pradhan, Developments of metal phosphides as efficient OER precatalysts. *J. Phys. Chem. Lett.* **8**, 144–152 (2017)
- P. Liu, J.A. Rodriguez, Catalysts for hydrogen evolution from the [NiFe] hydrogenase to the Ni₂P(001) surface: the importance of ensemble effect. *J. Am. Chem. Soc.* **127**, 14871–14878 (2005)
- H. Zhang, W. Zhou, J. Dong, X.F. Lu, X.W.D. Lou, Intramolecular electronic coupling in porous iron cobalt (oxy)phosphide nanoboxes enhances the electrocatalytic activity for oxygen evolution. *Energy Environ. Sci.* **12**, 3348–3355 (2019)
- Y. Li, H. Zhang, M. Jiang, Q. Zhang, P. He, X. Sun, 3D Self-supported Fe-doped Ni₂P nanosheet arrays as bifunctional catalysts for overall water splitting. *Adv. Funct. Mater.* **27**, 1–8 (2017)
- F. Yu, H. Zhou, Y. Huang, J. Sun, F. Qin, J. Bao, W.A. Goddard, S. Chen, Z. Ren, High-performance bifunctional porous non-noble metal phosphide catalyst for overall water splitting. *Nat. Commun.* **9**, 1–9 (2018)
- Q. Shi, Q. Liu, Y. Ma, Z. Fang, Z. Liang, G. Shao, B. Tang, W. Yang, L. Qin, X. Fang, High-performance trifunctional electrocatalysts based on FeCo/Co₂P hybrid nanoparticles for zinc-air battery and self-powered overall water splitting. *Adv. Energy Mater.* **10**, 1903854 (2020)
- Y. Xin, X. Kan, L.Y. Gan, Z. Zhang, Heterogeneous bimetallic phosphide/sulfide nanocomposite for efficient solar-energy-driven overall water splitting. *ACS Nano* **11**, 10303–10312 (2017)
- G. Zhao, Y. Jiang, S.X. Dou, W. Sun, H. Pan, Interface engineering of heterostructured electrocatalysts towards efficient alkaline hydrogen electrocatalysis. *Sci. Bull.* **66**, 85–96 (2021)
- X. Guo, X. Zheng, X. Hu, Q. Zhao, L. Li, P. Yu, C. Jing, Y. Zhang, G. Huang, B. Jiang, C. Xu, F. Pan, Electrostatic adsorbing graphene quantum dot into nickel-based layered double hydroxides: Electron absorption/donor effects enhanced oxygen electrocatalytic activity. *Nano Energy* **84**, 105932 (2021)
- P.F. Liu, X. Li, S. Yang, M.Y. Zu, P. Liu, B. Zhang, L.R. Zheng, H. Zhao, H.G. Yang, Ni₂P(O)/Fe₂P(O) interface can boost oxygen evolution electrocatalysis. *ACS Energy Lett.* **2**, 2257–2263 (2017)
- Y. Li, C. Zhao, Iron-doped nickel phosphate as synergistic electrocatalyst for water oxidation. *Chem. Mater.* **28**, 5659–5666 (2016)
- L. Wu, L. Yu, F. Zhang, B. McElhenny, D. Luo, A. Karim, S. Chen, Z. Ren, Heterogeneous bimetallic phosphide Ni₂P-Fe₂P as an efficient bifunctional catalyst for water/seawater splitting. *Adv. Funct. Mater.* **31**, 1–12 (2021)
- S. Liu, L. Zheng, P. Yu, S. Han, X. Fang, Novel composites of α-Fe₂O₃ tetrakaidecahedron and graphene oxide as an effective photoelectrode with enhanced photocurrent performances. *Adv. Funct. Mater.* **26**, 3331–3339 (2016)
- H. Zhang, A.W. Maijenburg, X. Li, S.L. Schweizer, R.B. Wehrspohn, Bifunctional heterostructured transition metal phosphides for efficient electrochemical water splitting. *Adv. Funct. Mater.* **30**, 1–31 (2020)
- Z. Xing, Q. Liu, A.M. Asiri, X. Sun, Closely interconnected network of molybdenum phosphide nanoparticles: a highly efficient electrocatalyst for generating hydrogen from water. *Adv. Mater.* **26**, 5702–5707 (2014)
- K. Fan, H. Chen, Y. Ji, H. Huang, P.M. Claesson, Q. Daniel, B. Philippe, H. Rensmo, F. Li, Y. Luo, L. Sun, Nickel-vanadium monolayer double hydroxide for efficient electrochemical water oxidation. *Nat. Commun.* **7**, 1–9 (2016)
- X. Liang, H.W. Zheng, X.J. Li, Y.H. Yu, G.T. Yue, W. Zhang, J.J. Tian, T.F. Li, Nanocomposites of Bi₅FeTi₃O₁₅ with MoS₂ as novel Pt-free counter electrode in dye-sensitized solar cells. *Ceram. Int.* **42**, 12888–12893 (2016)
- C.C.L. McCrory, S. Jung, J.C. Peters, T.F. Jaramillo, Benchmarking heterogeneous electrocatalysts for the oxygen evolution reaction. *J. Am. Chem. Soc.* **135**, 16977–16987 (2013)
- J. Lee, S.Y. Jun, T. Choi, D. Jung, J.S. Bae, S.A. Lee, W.S. Choi, Epitaxial strain dependent electrocatalytic activity in CaRuO₃ thin films. *Appl. Phys. Lett.* **117**, 163906 (2020)

33. M.S. Burke, L.J. Enman, A.S. Batchellor, S. Zou, S.W. Boettcher, Oxygen evolution reaction electrocatalysis on transition metal oxides and (oxy)hydroxides: activity trends and design principles. *Chem. Mater.* **27**, 7549–7558 (2015)
34. L. Yu, Q. Zhu, S. Song, B. McElhenny, D. Wang, C. Wu, Z. Qin, J. Bao, Y. Yu, S. Chen, Z. Ren, Non-noble metal-nitride based electrocatalysts for high-performance alkaline seawater electrolysis. *Nat. Commun.* **10**, 5106 (2019)
35. Y. Wu, Y. Yi, Z. Sun, H. Sun, T. Guo, M. Zhang, L. Cui, K. Jiang, Y. Peng, J. Sun, Bimetallic Fe-Ni phosphide carved nanoframes toward efficient overall water splitting and potassium-ion storage. *Chem. Eng. J.* **390**, 124515 (2020)
36. Y.J. Tang, L. You, K. Zhou, Enhanced oxygen evolution reaction activity of a Co₂P@NC-Fe₂P composite boosted by interfaces between a N-doped carbon matrix and Fe₂P microspheres. *ACS Appl. Mater. Interfaces* **12**, 25884–25894 (2020)
37. B. Zhang, Y.H. Lui, A.P.S. Gaur, B. Chen, X. Tang, Z. Qi, S. Hu, Hierarchical FeNiP@ultrathin carbon nanoflakes as alkaline oxygen evolution and acidic hydrogen evolution catalyst for efficient water electrolysis and organic decomposition. *ACS Appl. Mater. Interfaces* **10**, 8739–8748 (2018)
38. L. Zhang, C. Chang, C.W. Hsu, C.W. Chang, S.Y. Lu, Hollow nanocubes composed of well-dispersed mixed metal-rich phosphides in N-doped carbon as highly efficient and durable electrocatalysts for the oxygen evolution reaction at high current densities. *J. Mater. Chem. A* **5**, 19656–19663 (2017)
39. L. Zheng, W. Hu, X. Shu, H. Zheng, X. Fang, Ultrafine CoPx nanoparticles anchored on nitrogen doped reduced graphene oxides for superior hydrogenation in alkaline media. *Adv. Mater. Interfaces* **5**, 1800515 (2018)

Publisher's Note Springer Nature remains neutral with regard to jurisdictional claims in published maps and institutional affiliations.